Ultranarrow-Band Photon Pair Source Compatible with Solid State Quantum Memories and Telecommunication Networks

Julia Fekete,[1] Daniel Rieländer,[1] Matteo Cristiani,[1] and Hugues de Riedmatten[1, 2, *]

[1]*ICFO-The Institute of Photonic Sciences, Mediterranean Technology Park, 08860 Castelldefels, Spain*
[2]*ICREA-Institució Catalana de Recerca i Estudis Avançats, 08015 Barcelona, Spain*

We report on a source of ultranarrow-band photon pairs generated by widely nondegenerate cavity-enhanced spontaneous down-conversion. The source is designed to be compatible with Pr^{3+} solid state quantum memories and telecommunication optical fibers, with signal and idler photons close to 606 nm and 1436 nm, respectively. Both photons have a spectral bandwidth around 2 MHz, matching the bandwidth of Pr^{3+} doped quantum memories. This source is ideally suited for long distance quantum communication architectures involving solid state quantum memories.

The interaction between quantum light and matter has important implications in quantum information science because it forms the basis of quantum memories (QM) for light [1–4]. For applications in long distance quantum communication networks, it is required that QMs are connected to optical fibers. However, most QMs absorb photons at wavelengths very far from telecommunication wavelengths. To overcome this limitation, possible solutions include quantum frequency conversion [5] or entanglement between QMs and telecommunication photons via nondegenerate photon pair sources as proposed in [6].

Rare-earth doped solids have shown very promising characteristics as solid state QMs [4, 7]. Short lived entanglement between atomic excitations stored in rare-earth crystals and photons at telecommunication wavelength has been demonstrated recently [8, 9]. Among the many rare-earth elements, praseodymium (Pr^{3+}) doped solids possess, so far, the best demonstrated properties in terms of quantum storage. For example, a very high storage efficiency (up to 69%) has been demonstrated [10]. In addition, in contrast to the materials used in [8, 9], Pr^{3+} has a ground state structure with 3 long lived hyperfine levels, enabling long term light storage in spin states, with storage times > 1 s demonstrated for coherent light pulses [11].

Despite these exceptional properties, there is, so far, no quantum light source compatible with Pr^{3+} QMs. Instead, all experiments were done using either strong [11–13] or weak [10, 14, 15] coherent states of light. The main challenge in realizing such a light source is that the bandwidth of the memory is limited to a few MHz by the excited state spacing of the ions. In addition, as mentioned above, it would be desirable to have a photon pair source with one photon compatible with the QM and the other photon at telecommunication wavelength to minimize losses for long distance fiber transmission [6].

Spontaneous parametric down-conversion (SPDC) is an interesting candidate for realizing such a quantum light source. It is a standard technology and the phase-matching can be tailored to allow for the creation of photons at very different wavelengths. However, the frequency spectrum obtained in down-conversion (typically > 100 GHz) is several orders of magnitude larger than the bandwidth required to interact with Pr^{3+} doped QMs. One possibility for overcoming this problem is to spectrally filter the SPDC output [16]. This solution requires SPDC sources with large spectral brightness [16], such as nonlinear waveguides [8, 17] and several stages of filtering. Another possibility is to place the crystal inside an optical cavity, which enhances the probability of generating a photon pair in the resonant mode with respect to the single-pass case. Cavity-enhanced SPDC was first demonstrated in 1999 [18] and since then many experiments have been performed in various cavity designs [19–23]. Recently, atom-resonant photon pairs have been generated [24–26] and used for quantum storage [27] and quantum metrology application [28]. In most cavity-enhanced down-conversion experiments so far, the photons were frequency degenerate or close to degeneracy (with the exception of [22] where the wavelength difference was 100 nm). In nondegenerate cavity sources the enhancement of photon pair generation probability occurs only for a limited set of longitudinal modes, called clusters [21, 29]. This clustering effect has been recently proposed for engineering single-mode narrow-band sources [23, 30].

In this Letter, we report on an ultranarrow-band widely nondegenerate photon pair source compatible with Pr^{3+} doped QMs and with telecom optical fibers. The photon pairs are obtained by cavity-enhanced SPDC and have a wavelength near 606 nm (the resonant wavelength of $Pr^{3+} : Y_2SiO_5$ crystals, signal photon) and 1436 nm (idler photon). The measured correlation time of the pairs is 104 ns, the longest reported for a SPDC source to our knowledge, leading to single photon spectral bandwidths of $1.6 - 2.9$ MHz, matching the bandwidth of Pr^{3+} doped QMs. In addition, we show a strong reduction of the number of longitudinal modes emitted by the cavity due to the clustering effect, which facilitates the

filtering to obtain single-mode operation. Indeed, by inserting a properly designed filter for the signal photons, we obtain strong evidence of single-mode operation.
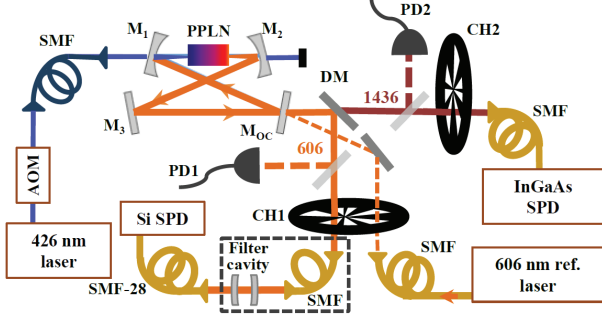

FIG. 1: Experimental setup. AOM, acousto-optic modulator; SMF, single-mode fiber; $M_{1,2,3}$ highly reflective mirrors; M_{OC} output coupler mirror; DM, dichroic mirror; PD1,2, photodiodes; CH1,2, choppers; SPD, single-photon detectors.

The scheme of the photon pair source is shown in Fig. 1. The pump for the down-conversion is a 426.2 nm single-frequency continuous-wave laser system (Toptica TA SHG). The pump light is passing through an acousto-optic modulator (AOM) that allows for varying the pump power incident on the cavity. After the AOM the light is coupled into a single-mode fiber (SMF) for spatial mode cleaning. The SPDC process is based on type I quasi-phase-matching in a 2 cm long periodically poled lithium niobate (PPLN) crystal (5 % MgO doped PPLN with 16.5 μm poling period, AR coated for 426, 606, 1436 nm, provided by HCPhotonics Corp.) The bow-tie cavity surrounding the crystal has finesse $\mathcal{F} \approx 200$, and free spectral range $FSR \approx 414$ MHz. The mirror reflectivities for signal and idler wavelength are 99.99% for $M_{1,2,3}$, and 98.5% for the output coupler (M_{OC}, Layertec GmbH).

In order to obtain enhancement of the photon pair generation probability, resonance for both the signal and idler frequencies has to be ensured. In addition, the signal frequency has to be resonant with Pr^{3+} : Y_2SiO_5 crystals. To achieve these conditions a complex lock system was implemented. A reference beam at 606 nm, resonant with Pr^{3+} ions [15], is coupled into the cavity through M_{OC}, copropagating with the pump beam. The reflection from the cavity is used for locking the cavity length at resonance with the signal frequency, by means of a piezo element moving M_{OC}. A reference beam at the idler frequency is obtained by difference-frequency generation between the pump (426 nm) and the 606 nm reference beam and is used for locking the pump frequency to maintain double resonance. The lock system is acting during 45% of the total operation time, alternating with the measurement time, separated by mechanical choppers (CH1,2). During the measurement time, no classical reference signal beam is present in the cavity to protect the single-photon detectors (SPD) and

avoid excessive noise. The down-converted photons are spectrally filtered, fiber coupled (SMF-28: single-mode at 1436 nm, and slightly multimode at 606 nm) and detected by SPDs (Si SPD: Perkin Elmer SPCM-AQR-16-FC with detection efficiency, $\eta_{det,606} \approx 60$ %; InGaAs SPD: IdQuantique id220 used in free-running mode with $\eta_{det,1436} \approx 10-20$ %). The measured transmission from the output of the cavity to the SPDs is 0.46 (0.31) for the signal (idler) photons.

The quantum state of the emitted photon pairs can be analyzed by the second-order cross-correlation function between the signal and idler fields, $G_{s,i}^{(2)}(\tau)$ - see appendix for details. To do so, the frequency nondegenerate photons of the pair are spatially separated by a dichroic mirror (DM) and their arrival times at the detectors are recorded by a time-to-digital-converter card (Signadyne). To create the correlation function, the arrival-time differences (τ) are plotted in a histogram, as shown in Fig. 2(a).
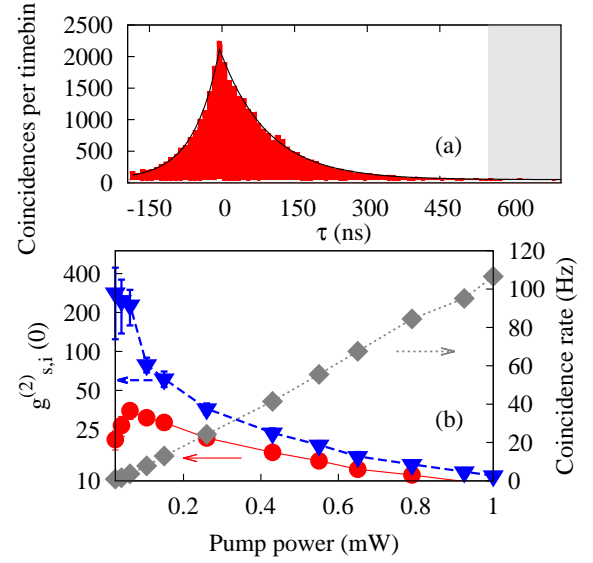

FIG. 2: Measured correlation functions of the unfiltered photon pair source. (a) $G_{s,i}^{(2)}(\tau)$ function (measured at 130 μW pump power, $\eta_{det,1436} = 10$ %, 43 min integration time, 10 ns time-bin size). The dark count rate (light-gray bars of values below 50) is obtained by blocking the InGaAs SPD. $g_{s,i}^{(2)}(0)$ is calculated using the fit function (solid line) as the peak value divided by the accidental region (shaded area) average count rate level. (b) Power dependence of $g_{s,i}^{(2)}(0)$ without and with dark count subtraction (left axis, circles and triangles, respectively) and coincidence count rates (right axis, diamonds).

We observe a FWHM correlation time of 104 ns, which, to our knowledge, is the highest value reported from a SPDC source so far. The double exponential decay of $G_{s,i}^{(2)}(\tau)$ is due to the photon lifetime inside the cavity and allows for the estimation of the cavity linewidth, $\Delta\nu$. Fitting $\exp(-2\pi\Delta\nu\tau)$ on the two sides of the correlation function results in $\Delta\nu = 1.7$ MHz at 1436 nm and

2.9 MHz at 606 nm. The asymmetry is a clear sign of the difference of the finesse for the two wavelengths which can be explained by a slight difference in the reflectivities of the mirrors or the crystal surfaces. From these values we infer internal cavity losses of $1 - 2.5\,\%$ and cavity escape efficiencies of $\sim 0.6 - 0.4$ [31].

To further characterize the source, the histograms were measured at various pump power levels. The number of total coincidences within a $500\,\mathrm{ns}$ time window increases linearly with pump power [see Fig. 2(b)]. The detected pair production rate after dark count subtraction is $C = 100\,\mathrm{Hz/mW}$. For applications in quantum information science, another critical parameter is the normalized cross-correlation function at zero delay, $g_{s,i}^{(2)}(0)$, which is also plotted in Fig. 2(b) as a function of pump power. In order to obtain good fidelities in quantum protocols, high $g_{s,i}^{(2)}(0)$ is needed. As expected, $g_{s,i}^{(2)}(0)$ is inversely proportional to the pump power [22]. Without subtracting any background, we reach values of $g_{s,i}^{(2)}(0)$ up to 35, significantly higher than the classical threshold of 2 for two-mode squeezed states. For a pump power of $1\,\mathrm{mW}$, we still observe $g_{s,i}^{(2)}(0) = 9.3$. At very low power (below $100\,\mu\mathrm{W}$) the measurements are limited by dark counts, reducing $g_{s,i}^{(2)}(0)$ [32]. The $g_{s,i}^{(2)}(0)$ with dark count subtraction (also plotted) approaches a value of 284 at $24\,\mu\mathrm{W}$, showing the high purity of our photon pair source.

As a possible application of the photon pair source, the telecom photons could be used to herald the presence of the signal photons to be absorbed by the QM. To give an estimate for the heralding efficiency (η^H), the singles count rate at the InGaAs SPD (S_{1436}) has to be taken into account, resulting in $\eta^H = C/S_{1436}/\eta_{\mathrm{det},606} = 13\,\%$.

We now investigate the spectral content of the emitted photons. Compared to the single-pass SPDC, where the spectrum is determined by the phase-matching bandwidth (FWHM $\approx 80\,\mathrm{GHz}$ in our case), for cavity-enhanced SPDC the spectrum is modified by the cavity modes. Since the signal and idler have different dispersion characteristics, the respective FSRs also differ, and the joint spectral amplitude will consist of spectral modes restricted to certain clusters [29, 30]. The cluster spacing and width are determined by the dispersion relations and the cavity geometry. A first insight on the spectral content of the emitted photons can be inferred from the $G_{s,i}^{(2)}(\tau)$ function. As shown in Fig. 3(a), the histogram taken with 325 ps timebin size shows an oscillatory behavior. This is the consequence of the presence of multiple spectral modes [19]. The periodicity follows the cavity round-trip time ($T = 1/FSR = 2.4\,\mathrm{ns}$), as the photon wave packet incorporates the beating from several frequency components spaced by the FSR. From the temporal width of the peaks ($\sim 880\,\mathrm{ps}$) and taking into account the time resolution of the detection system ($\sim 685\,\mathrm{ps}$), we infer that the spectrum is composed of

clusters containing around 4 longitudinal modes (see appendix). This technique is, however, limited to a few GHz by the detection time resolution.

To further investigate the presence of multiple modes we measured the first order autocorrelation (coherence) function of the signal photons, $V = |g_s^{(1)}(\Delta t)|$, in a 100 ps range using a Michelson interferometer [33]. This was obtained by measuring the visibility V of the interference fringes as a function of the time difference Δt between the two arms of the interferometer. To vary the path length difference, one of the mirrors was placed on a translation stage together with a piezo element for fine tuning. The results are shown in Fig. 3(b).
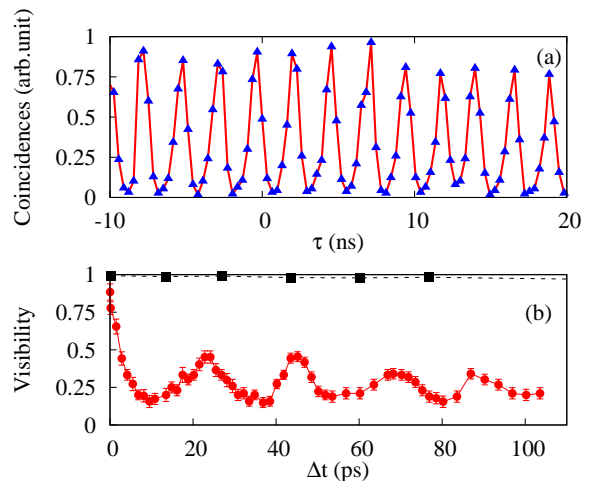

FIG. 3: Temporal oscillations in the correlation functions for the unfiltered photon pair source. (a) Zoom of the $G_{s,i}^{(2)}(\tau)$ function of Fig. 2(a) to the $-10 - 20$ ns region evaluated with 325 ps time-bin size. (b) $|g_s^{(1)}(\Delta t)|$ function (circles). As reference, the visibility for classical light is shown (squares).

The oscillations that we observe in the $|g_s^{(1)}(\Delta t)|$ function can be understood from the clustering effect. From the 22.5 ps oscillation period, we can infer the presence of clusters separated by 44.5 GHz. From the calculated phase-matching bandwidth, we infer that at most 3 clusters are present. During the locking period the main cluster is centered in the vicinity of the peak of the phase-matching curve. The contrast of the oscillations (~ 0.4) is compatible with a suppression of more than 80 % of the side clusters. The interference visibility for the oscillation peaks is reduced to $\sim 45\,\%$, which can be explained by the presence of broadband noise that was not eliminated properly.

The multimode cavity could in principle be used as the source for storage of several longitudinal modes within the inhomogeneous absorption line of a Pr^{3+} QM, to implement frequency multiplexing. Nevertheless, in absence of a frequency multimode QM, it is important to show that our source can also operate in the single-mode regime. To achieve this, we inserted a filter cavity (FC) in
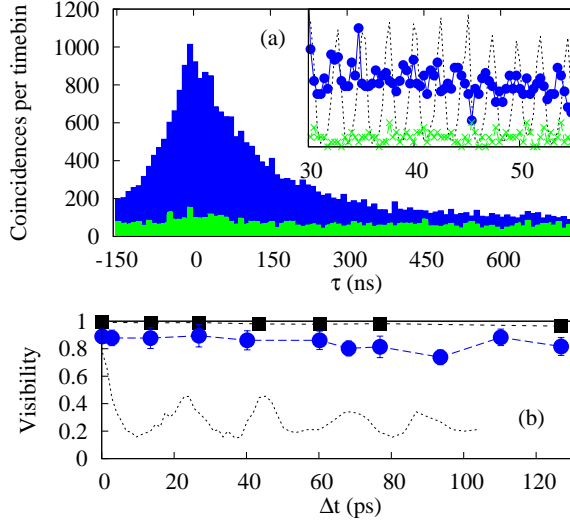
FIG. 4: Measured correlation functions of the cavity output when the signal was spectrally filtered. (a) $G_{s,i}^{(2)}(\tau)$ function (1.7 mW pump power, $\eta_{\det,1436} = 20\%$, 60 min integration time, 10 ns time-bin size). The noise level [light-gray (green in color version) bars] was measured with FC off-resonant with the signal. The inset is a zoom to the $30 - 55$ ns region evaluated with 325 ps time-bin size. The dashed line corresponds to the unfiltered case for comparison. (b) $|g_s^{(1)}(\Delta t)|$ function measured with 606 nm down-converted photons after dark count subtraction (circles). As reference, the visibility for classical light (squares), and for the unfiltered cavity (dotted line) are plotted.

the 606 nm arm, designed to suppress all modes around the fundamental one. The FSR was chosen such that the transmission peaks do not coincide with the neighboring clusters ($\Delta\nu = 80$ MHz, $FSR = 16.8$ GHz). The FC transmission for long term measurements was 11 %, including a peak transmission of 22 % (fiber-to-fiber) and a further drop of 50 % due to frequency drifts of the only passively stabilized FC. For this measurement, a single-mode fiber was inserted in the signal arm [with reduced fiber coupling compared to the unfiltered cavity experiments ($\eta_C = 0.5$ and 0.8, respectively)].

The measured $G_{s,i}^{(2)}(\tau)$ function of the signal transmitted by the FC and the unfiltered idler is plotted in Fig. 4(a). We obtain a raw $g_{s,i}^{(2)}(0)$ of 9. Note that a significant part of accidental coincidences are due to the fact that only the signal photon is filtered. The number of coincidences (500 ns window) with the background level subtracted is 2.9 Hz/mW. Comparing this with the unfiltered cavity–correcting for the different experimental conditions–we find a reduction of ~ 4.5 for the coincidence rate which is consistent with the number of modes estimated from the unfiltered experiment.

The suppression of the oscillations at 2.4 ns for the filtered signal [inset of Fig. 4(a)] confirms the suppression of neighboring spectral modes within the same cluster. The

suppression of modes in the neighboring clusters was also tested by measuring the $|g_s^{(1)}(\Delta t)|$ for the filtered signal, see Fig. 4(b). The visibility is above 80% over the 120 ps range (average $\sim 88 \pm 5\%$) and there is no sign of decay over this range. This leads to the conclusion that the neighboring clusters were also suppressed efficiently. The combination of $G_{s,i}^{(2)}(\tau)$ and $|g_s^{(1)}(\Delta t)|$ measurements is strong evidence of the presence of a single spectral mode in the signal. Note that only a single filtering stage is needed to reach the single-mode regime.

The spectral brightness corresponding to the probability of finding a pair in single-mode fibers (i.e. correcting only for detection efficiencies) for the filtered source is 11 pairs/ (s · mW · MHz). Correcting for all known losses after the creation of the photon pair we find 8×10^3 pairs/ (s · mW · MHz), which shows that passive loss is a major issue to be improved. Compared with the single-pass case, where we measure a coincidence rate of 3000 Hz/mW (for $\eta_{\det,1436} = 0.1$), the cavity enhances the spectral brightness by $B = 1250$ [18] (correcting for filter transmission, cavity escape efficiencies, and chopper duty cycle).

In conclusion, we have demonstrated a quantum light source that is suitable to connect solid state Pr^{3+} QMs to fiber optics networks. This is an important step towards long distance quantum repeaters using solid state QMs. Beyond this application, our source is also a proof-of-principle that cavity-enhanced down-conversion can be used as a versatile source of narrow-band photon pairs at widely separated wavelengths, which is relevant in the context of connecting light-matter quantum interfaces of different kinds.

Appendix: Evaluation of the second-order cross-correlation function

The normalized form of $G_{s,i}^{(2)}(\tau)$, the second-order cross-correlation function between signal and idler fields $(E_{s,i})$, can be expressed as:

$$g_{s,i}^{(2)}(\tau) \equiv \frac{\langle E_s^\dagger(t) E_i^\dagger(t+\tau) E_i(t+\tau) E_s(t) \rangle}{\langle E_i^\dagger(t+\tau) E_i(t+\tau) \rangle \langle E_s^\dagger(t) E_s(t) \rangle}, \quad (1)$$

Following the theory used in [25, 26], in the case of doubly-resonant cavity-enhanced downconversion it

takes the form:

$$g_{s,i}^{(2)}(\tau) \propto \left| \sum_{m_s,m_i=0}^{\infty} \frac{\sqrt{\gamma_s\,\gamma_i\,\omega_s\,\omega_i}}{\Gamma_s + \Gamma_i} \right.$$
$$\left. \times \begin{cases} e^{-2\pi\Gamma_s(\tau-(\tau_0/2))}\mathrm{sinc}(i\pi\tau_0\Gamma_s) & \tau \geqslant \frac{\tau_0}{2} \\ e^{+2\pi\Gamma_i(\tau-(\tau_0/2))}\mathrm{sinc}(i\pi\tau_0\Gamma_i) & \tau < \frac{\tau_0}{2} \end{cases} \right|^2,$$
$$(2)$$

where $\gamma_{s,i}$ are the cavity damping rates for signal and idler, $\omega_{s,i}$ are the central frequencies, $\Gamma_{s,i} = \gamma_{s,i}/2 + im_{s,i}FSR_{s,i}$ with mode indices $m_{s,i}$ and free spectral ranges $FSR_{s,i}$, and τ_0 is the transit time difference between the signal and idler photons through the SPDC crystal.
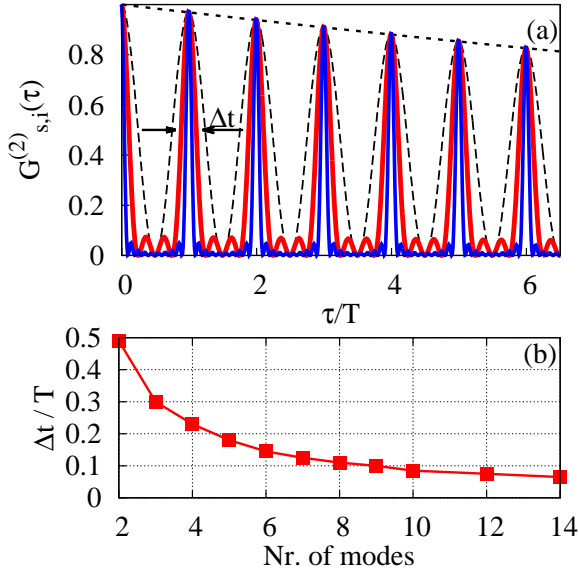

FIG. 5: Dependence of the $G_{s,i}^{(2)}(\tau)$ function on the number of spectral modes. (a) Correlation functions for 1, 2, 4, and 10 modes (dotted, dashed, thick solid, and thin solid lines, respectively). (b) Width of the oscillation peaks versus the number of modes.

In Fig. 5(a) simulated $G_{s,i}^{(2)}(\tau)$ functions are plotted as a function of time delay (τ) normalized to the cavity roundtrip time (T). The different curves correspond to different number of spectral modes taken into account. As the number of modes is increased, the superposition of the sinc functions results in the oscillation peak width's (Δt) reduction. This effect is also shown in Fig. 5(b). Taking into account the time resolution of our detection system ($\sim 685\,\mathrm{ps}$) we can estimate the expected temporal width of the peaks by convolution. From the best agreement when changing the number of modes we infer that the spectrum is composed of clusters containing around 4 longitudinal modes (peak width $\sim 880\,\mathrm{ps}$). Note that this corresponds to 4 modes of equal height, which is phys-

ically not the case, but their contribution to the peak width should be similar.

---

* Electronic address: hugues.deriedmatten@icfo.es
[1] K. Hammerer, A. S. Sørensen, and E. S. Polzik, Rev. Mod. Phys. **82**, 1041 (2010).
[2] C. Simon *et al.*, Eur. Phys. J. D **58**, 1 (2010).
[3] A. I. Lvovsky, B. C. Sanders, and W. Tittel, Nat. Photon. **3**, 706 (2009).
[4] N. Sangouard, C. Simon, H. de Riedmatten, and N. Gisin, Rev. Mod. Phys. **83**, 33 (2011).
[5] A. G. Radnaev *et al.*, Nat. Phys. **6**, 894 (2010).
[6] C. Simon *et al.*, Phys. Rev. Lett. **98**, 190503 (2007).
[7] W. Tittel *et al.*, Laser & Photonics Rev. **4**, 244 (2010).
[8] C. Clausen *et al.*, Nature (London) **469**, 508 (2011).
[9] E. Saglamyurek *et al.*, Nature (London) **469**, 512 (2011).
[10] M. P. Hedges, J. J. Longdell, Y. Li, and M. J. Sellars, Nature (London) **465**, 1052 (2010).
[11] J. J. Longdell, E. Fraval, M. J. Sellars, and N. B. Manson, Phys. Rev. Lett. **95**, 063601 (2005).
[12] M. Afzelius *et al.*, Phys. Rev. Lett. **104**, 040503 (2010).
[13] G. Heinze, S. Mieth, and T. Halfmann, Phys. Rev. A **84**, 013827 (2011).
[14] M. Sabooni *et al.*, Phys. Rev. Lett. **105**, 060501 (2010).
[15] M. Gündoğan, P. M. Ledingham, A. Almasi, M. Cristiani, and H. de Riedmatten, Phys. Rev. Lett. **108**, 190504 (2012).
[16] A. Haase, N. Piro, J. Eschner, and M. W. Mitchell, Opt. Lett. **34**, 55 (2009).
[17] I. Usmani *et al.*, Nat. Photon. **6**, 234 (2012).
[18] Z. Y. Ou and Y. J. Lu, Phys. Rev. Lett. **83**, 2556 (1999).
[19] H. Wang, T. Horikiri, and T. Kobayashi, Phys. Rev. A **70**, 043804 (2004).
[20] C. E. Kuklewicz, F. N. C. Wong, and J. H. Shapiro, Phys. Rev. Lett. **97**, 223601 (2006).
[21] E. Pomarico *et al.*, New J. Phys. **11**, 113042 (2009).
[22] M. Förtsch, J. Fürst, C. Wittmann, D. Strekalov, A. Aiello, M. V. Chekhova, C. Silberhorn, G. Leuchs, and C. Marquardt, arXiv:1204.3056v3.
[23] C.-S. Chuu, G. Y. Yin, and S. E. Harris, Appl. Phys. Lett. **101**, 051108 (2012).
[24] X.-H. Bao *et al.*, Phys. Rev. Lett. **101**, 190501 (2008).
[25] M. Scholz, L. Koch, and O. Benson, Phys. Rev. Lett. **102**, 063603 (2009).
[26] F. Wolfgramm, Y. A. de Icaza Astiz, F. A. Beduini, A. Cerè, and M. W. Mitchell, Phys. Rev. Lett. **106**, 053602 (2011).
[27] H. Zhang *et al.*, Nat. Photon. **5**, 628 (2011).
[28] F. Wolfgramm, C. Vitelli, F. A. Beduini, N. Godbout, and M. W. Mitchell, Nat. Photon. **7**, 28 (2013).
[29] Y. Jeronimo-Moreno, S. Rodriguez-Benavides, and A. B. U'Ren, Laser Phys. **20**, 1221 (2010).
[30] E. Pomarico *et al.*, New J. Phys. **14**, 033008 (2012).
[31] F. Wolfgramm, Ph. D. thesis, ICFO-The Institute of Photonic Sciences, 2011.
[32] P. Sekatski *et al.*, J. Phys. B **45**, 124016 (2012).
[33] F.-Y. Wang, B.-S. Shi, C. Zhai, and G.-C. Guo, J. Mod. Opt. **57**, 330 (2010).